An Improved Model Predictive Current Control for PMSM Drives Based on Current Track Circle

Xiaodong Sun, *Senior Member, IEEE*, Minkai Wu, Gang Lei, *Member, IEEE*, Youguang Guo, *Senior Member, IEEE*, and Jianguo Zhu, *Senior Member, IEEE*

***Abstract*—Model predictive current control (MPCC) is a high-performance control strategy for permanent magnet synchronous motor (PMSM) drives, with the features of quick response and simple computation. However, the conventional MPCC results in high torque and current ripples. This paper proposes an improved MPCC scheme for PMSM drives. In the proposed scheme, the back electromotive force is estimated from the previous stator voltage and current, and it is used to predict the stator current for the next period. To further improve the steady state and dynamic performance, the proposed MPCC selects the optimal voltage vector based on a current track circle instead of a cost function. Compared with the calculation of cost function, the prediction of the current track circle is simple and quick. The proposed MPCC is compared with conventional MPCC and a duty-circle based MPCC (DCMPCC) by simulation and experiment in the aspect of converter output voltage and sensitivity analysis. Results prove the superiority of the proposed MPCC and its effectiveness in reducing the torque and current ripples of PMSM drives.**

***Index terms*- Permanent magnet synchronous motor, model predictive current control, current track circle, cost function**

I. INTRODUCTION

A. Motivation

Recently the environment is getting more and more concerned due to the use of fossil fuels without restraint. The most prominent application is the tradition fuel vehicles, and it is time to upgrade and update. Electrical vehicles (EVs) have less emission and higher energy conversion efficiency [1]-[5]. With the advantages of high efficiency, high power density, small size and light weight, the permanent-magnet synchronous motors (PMSMs) are considered as new power source applied in EVs to replace the internal combustion engine [6] and [7]. The EVs motor should have a large starting torque and a wide range of speed regulation ability to meet the required power and torque of starting, acceleration, driving, deceleration and braking. In addition, the motor also needs high controllability, steady precision and dynamic performance. Therefore, an efficient and advanced control strategy is necessary to improve the drive performance of PMSMs.

Manuscript received August 09, 2019; revised January 6, 2020; accepted March 12, 2020. This work was supported by the National Natural Science Foundation of China under Project 51875261, the Natural Science Foundation of Jiangsu Province of China under Projects BK20180046 and BK20170071, the "Qinglan project" of Jiangsu Province, the Key Project of Natural Science Foundation of Jiangsu Higher Education Institutions under Project 17KJA460005, and the Six Categories Talent Peak of Jiangsu Province under Project 2015-XNYQC-003. (*Corresponding author: Gang Lei*.)

X. Sun and M. Wu are with the Automotive Engineering Research Institute, Jiangsu University, Zhenjiang 212013, China (email: xdsun@ujs.edu.cn, ujswmk@163.com).

G. Lei and Y. Guo are with the School of Electrical and Data Engineering, University of Technology Sydney, NSW 2007, Australia (e-mail: Gang.Lei@uts.edu.au, Youguang.Guo-1@uts.edu.au).

J. Zhu is with the School of Electrical and Information Engineering, University of Sydney, NSW, 2006, Australia (e-mail: jianguo.zhu@sydney.edu.au).

B. Related Research

There are various kinds of control methods for PMSM drives, such as the field-oriented control (FOC) and direct torque control (DTC) [8], [9]. Although the FOC can achieve good steady-state performance and quick response with a wide speed range, it has difficulty in adapting the complicated vehicle motor conditions [10]. FOC consists of an internal current loop and an external speed loop which need fine tuning work. The stationary reference frame needs to transform to the rotating reference frame. In general, internal current loop and external speed loop are PI control modules [11]. In the DTC scheme, the current loop and pulse width modulation (PWM) block are not needed. And the final voltage vector is obtained from the pre-switch table on the basis of the torque and flux error signs. Compared to the FOC [12] and [13], the DTC has quicker dynamic response with simple structure. However, the DTC generates high torque and flux ripples and high switching frequency causes the hardware power loss [14] and [15]. The conventional FOC and DTC have been combined with sliding mode control to overcome the drawbacks.

With the increasing demands of electric drive system and recent advancements in the digital signal processing area, model predictive control (MPC) comes into reality as an efficient control scheme [16]. The PMSM, converter and controller compose the electric drive system to build model. MPC predicts the next period behavior of controlled variables, which are current, torque and stator flux. Different from DTC pre-switch, the MPC selects the optimal voltage vector by minimizing the error between the reference value and predictive value. A finite-control-set model predictive control (FCS-MPC) in [17] is applied. Hence, MPC is more precise and more efficient than DTC. A predictive speed controller (PSC) based on MPC was proposed in [18]. A dynamic performance with direct PSC has been achieved with short prediction horizon and less computational requirements. Model predictive torque control (MPTC) is an improved MPC which pays attention to high-performance torque control [19]. Usually, torque and stator flux are chosen as the control variables in the cost function. As for the torque ripple and current harmonics, MPTC demonstrates better performance than DTC [20]. Because of the

different units of torque and stator flux, the cost function focuses on weighting factor of stator flux which requests some tuning works and keeps the MPTC unique. Meanwhile, an improved model predictive current control (MPCC) based on the incremental model for PMSM drive was proposed in [21] to solve the parameter dependence problem. Two MPCC methods with a duty-cycle-control were proposed to achieve optimal vector selection and vector duration in [22]. In [23], an MPCC with phase-shifted pulse width modulation (PS-PWM) was presented to improve the steady-state control performance. Furthermore, a model-free predictive current control (PCC) of interior permanent-magnet synchronous motor (IPMSM) drive systems based on a current difference detection technique was proposed in [24]. Its computational load is relatively low and it is insensitive to parameter variations. In order to reduce the computation burden and eliminate the weighting factor in conventional model predictive torque control (MPTC), this paper proposed an improved MPTC algorithm without the use of weighting factor [25]. Nevertheless, the conventional MPCC usually employs only one voltage vector during one control period which is unable to obtain satisfactory performance because the current error does not reach the smallest. Being similar to DTC, the improved MPCC employs this principle that applies one active vector and one zero vector during one control period to produce small current variations. Therefore, MPCC can achieve higher steady-state performance and quicker response to a greater extent. A DFCB-MPTC was proposed in [26] to compensate the lumped disturbance by the analysis of FCS-MPTC with mismatched parameters and active disturbance ability of traditional PI controller. A continuous voltage vector model-free predictive current control method was proposed for surface-mounted PMSMs to reduce the current ripples of FCS-MPC in [27]. Reference [28] proposed a constant switching frequency multiple-vector based FCS-MPCC scheme to reduce computation burden, low-order harmonic currents, and variable switching frequencies. A generalized multiple-vector-based MPC for PMSM drives, which unifies the prior MPC methods in one frame with much lower complexity and computational burden proposed in [29]. These works made contribution to the computational complexity of duty-cycle-based MPCC indeed.

C. Contribution

This paper proposes an improve MPCC which selects the optimal voltage vector based on a current track circle instead of a cost function. The back electromotive force (EMF) is estimated based on the previous value of stator voltage and current. Furthermore, the sensitivity of motor parameter variations is verified. The main contributions of this paper are listed as follows.

1) The proposed MPCC establishes a new reference frame based on a current track circle. The current locus and initial points are shown in the established reference frame. Only one zero voltage must be predicted as to reduce the torque ripple and current harmonics instead of all the voltage vectors.
2) The proposed MPCC selects the optimal voltage vector based on a current track circle instead of a cost function to reduce the computational burden compared to the conventional MPCC and the duty-cycle-based MPCC (DCMPCC).

D. Paper organization

The remainder of this paper is organized as follows. Section II presents the model of PMSM and conventional MPCC. The proposed MPCC is given in Section III. Section IV describes the simulation results. Section V presents the experimental results and discussions, followed by the conclusion.

II. PMSM Model and Conventional MPCC

The continuous-time model of PMSM in the α-β-axis stationary reference rotor frame can be written as [19]

$$u_s = R_s i_s + \frac{d\psi_s}{dt} = R_s i_s + L_s \frac{di_s}{dt} + \frac{d\psi_x}{dt} = R_s i_s + L_s \frac{di_s}{dt} + E_x \quad (1)$$

$$\psi_x = \left[\psi_f + i_d (L_d - L_q)\right] e^{j\theta_e} \quad (2)$$

$$T_e = \frac{3}{2} p_n (\psi_x \otimes i_s) \quad (3)$$

where u_s, i_s, ψ_s, ψ_x, and $E_x = [E_\alpha\ E_\beta]^T$ represent the stator voltage vector, stator current vector, stator flux vector, active flux vector and back EMF, respectively. i_d and i_q denote the d-axis and q-axis current in the synchronous frame. R_s, L_d, L_q, ψ_f, and θ_e are the stator resistance, d-axis and q-axis inductance, permanent magnet flux, and electrical rotor position, respectively. T_e is the electromagnetic torque, and p_n is the number of pole pairs.

The equation of mechanical motion is expressed as

$$J \frac{d\omega_m}{dt} = T_e - T_l - B\omega_m \quad (4)$$

where J is the rotational inertia, B is the damping coefficient, ω_m is the mechanical angular velocity, and T_l is the load torque.

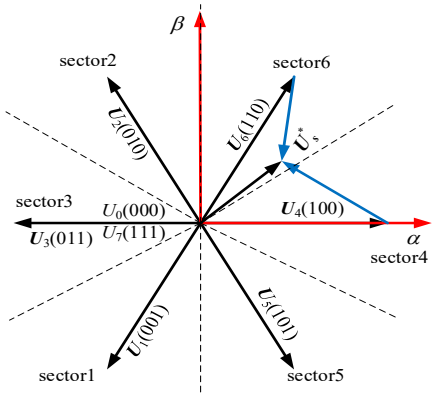

Fig. 1. Space voltage vector of a two-level voltage source inverter.

Considering the output form of power inverters, the predictive control strategies applied in the field of PMSM control are mostly based on the limited possible switching states, and the motor model is derived to predict the system behavior when various switching states are switched. As for the output of the predictive control algorithm, that is to say, the selection of switch state is always based on the control target. By defining a cost function composed of cost variables and comparing the future state value calculated based on the prediction model, the control output is obtained by minimizing the cost function value. Therefore, the predictive control strategy can be summarized into three parts, the definition of the cost function established according to the control objective,

discrete modeling of the motor control system and the output sequence of the system model which may be calculated based on the inverter state prediction model. Fig. 1 shows the voltage vectors of a two -level voltage source inverter in a stationary reference frame α-β.

The conventional MPCC relies on the minimization of a cost function to select the voltage vector. In other words, the cost function is on behalf of evaluation objectives to select the optimal voltage vector for the next sampling time. The winding current equation is discretized based on sampling time T_s. Using discrete time model, the future state set of winding current can be predicted according to the actual current measured at sampling time k in the prediction algorithm. The scheme of conventional MPCC is shown in Fig. 2.

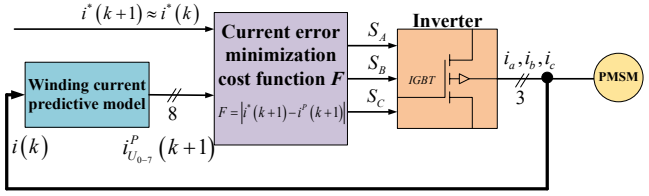

Fig. 2. Conventional MPCC control scheme.

The model predictive current control aims to stabilize the current signal and minimize the error between the predicted current value and the reference current value by calculating the cost function. The cost function can be expressed as follows:

$$F=\left|i_\alpha^*(k+1)-i_\alpha^P(k+1)\right|+\left|i_\beta^*(k+1)-i_\beta^P(k+1)\right| \quad (5)$$

where i_α and i_β are the real and imaginary components of the stator current in the stator reference frame, respectively. The values with superscript * and p represent reference and predicted values.

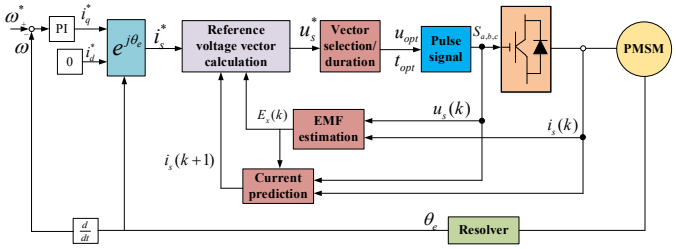

Fig. 3. DCMPCC control scheme.

In the duty-cycle-based MPCC (DCMPCC), as proposed MPCC II in [22], the reference voltage vector u_s^* is calculated as follows:

$$u_s^*=R_s i_s(k+1)+L_s\frac{i_s^*-i_s(k+1)}{T_s}+E_x(k) \quad (6)$$

As usual, the reference voltage vector u_s^* will be compounded by two nonzero voltage vectors and one zero with high switching frequency. In order to reduce the computational complexity and switching frequency, the DCMPCC only uses one nonzero voltage and one zero vector. The scheme of DCMPCC is shown in Fig. 3. On the basis of the location of u_s^*, it is time to select the optimal vector which is closest to the u_s^*. As shown in Fig. 1, the distance between u_6 and u_s^* is the shortest in all other nonzero voltages. Therefore, u_6 is selected as the optimal voltage vector. In other words, as soon as the location of u_s^* is ensured, the best nonzero voltage vector can be obtained, which is more efficient than the conventional MPCC.

The optimal duration of the best nonzero vector u_{opt} is also called duty circle and the cost function is established to guarantee the accuracy of selected voltage vector. The cost function is shown as follows:

$$F_1=\left|u_s^*-\frac{u_{opt}t_{opt}}{T_s}\right|^2 \quad (7)$$

By solving the derivation of F_1 in allusion to t_{opt}, the optimal vector duration is obtained as:

$$t_{opt}=\frac{u_s^*\cdot u_{opt}}{\left|u_{opt}\right|^2}T_s \quad (8)$$

It is evident that the selection of optimal voltage vector and duration are much simpler.

III. The Proposed MPCC

This study proposes a novel MPCC algorithm to simplify the control complexity and computational burden, which is based on a current track circle. The cost function is not needed because the current trajectory is corresponding with different voltage vector directions.

A. EMF Estimation

From (1), the current equation of PMSM can be obtained as follows:

$$\frac{di_s}{dt}=\frac{1}{L_s}\left(u_s-R_s i_s-E_x\right) \quad (9)$$

The derivative of current is discretized by using the forward Euler formula.

$$\frac{di_s}{dt}\approx\frac{i_s(k+1)-i_s(k)}{T_s} \quad (10)$$

$$i_s(k+1)=i_s(k)+\frac{T_s}{L_s}(u_s(k)-R_s i_s(k)-E_x(k)) \quad (11)$$

where T_s is the sampling time.

Due to the technology limitations, the back $E_x(k)$ cannot be directly measured. Fortunately, $E_x(k)$ can be calculated by (1) and (2), but it is strictly related to the accuracy of electrical parameters. Due to the variation of operating environment, the motor parameters have a large difference between the original parameters. Therefore, it is necessary to estimate the EMF directly using as few parameters as possible. During several control periods, the motor speed changes, which may be considered as that the speeds are approximate at k moment and (k+1)th moment. The $E_x(k)$ is concerned with the rotor speed ω, so E_x in several period can be assumed the same. According to the above analysis, the EMF at (k-1)th moment using the past values of stator voltage and current is:

$$E_x(k-1)=u_s(k-1)-R_s i_s(k)-\frac{L_s}{T_s}(i_s(k)-i_s(k-1)) \quad (12)$$

$$E_x(k)=\frac{1}{4}(E_x(k-1)+E_x(k-2)+E_x(k-3)+E_x(k-4)) \quad (13)$$

The similar EMF can be obtained at (k-2)th, (k-3)th and (k-4)th moment by the analogical method, respectively.

In simple terms, the predictive current in (11) can be deduced by the past value of estimated EMF in (12). The availability has been proved by the presented experimental results in [21]. However, the variations of inductance have

caused a fairly large error on the estimated EMF by the (12). In order to improve the stability and fault tolerance against the inductance variation, this paper uses the mean value of estimated EMFs during the last four control periods. Even if the inductance changes more than ±50%, the system is still stable and the estimated EMF is accurate.

B. One-step Delay Compensation

The final control of electrical motor drives is realized by the hardware and peripheral circuit. Because of the effect of various factors, the controller output cannot be applied immediately. For example, the required voltage vector obtained at (k)th moment is not implemented at (k+1)th moment due to the delay of the digital signal processors. Especially, the control performance is deteriorated when the number of samples is not high. Therefore, it is necessary to take action to compensate for the delay using the Heun's method. The accuracy of predictive current value in (11) will be lower than that of current prediction with new compensation method. The current compensation can be demonstrated as follows:

$$i_s^c(k+1) = i_s(k) + \frac{T_s}{L_s}(u_s(k) - R_s i_s(k) - E_x(k)) \tag{14}$$

$$i_s(k+1) = i_s^c(k+1) + \frac{-R_s(i_s^c(k+1) - i_s(k))T_s}{2L_q} \tag{15}$$

where $i_s^c(k+1)$ is the current compensation of stator current.

C. Selection of the Optimal Voltage Vector

This paper proposes an improved MPCC which selects the optimal voltage vector based on a current track circle instead of a cost function. After having obtained the back EMF from (12) and (13), the current at the next control period can be predicted by (14) and (15). The proposed MPCC predicts one zero voltage vector to achieve switching state for every sample period based on the direction of the current trajectory in a new reference frame. The control diagram of the proposed MPCC is shown in Fig. 4.

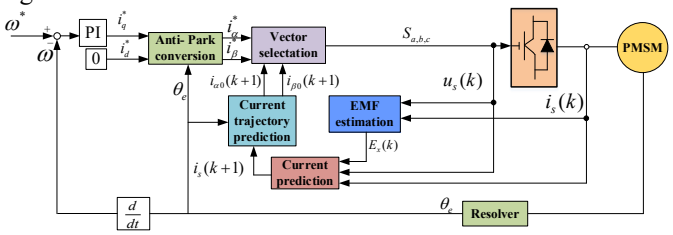

Fig. 4. Control diagram of the proposed MPCC.

Different from the conventional MPCC, the proposed MPCC cancels the cost function and builds the current track circle in the reference frame. The current equation is transformed into the following:

$$\begin{cases} \Delta i_\alpha(k+1) = \dfrac{T_s}{L_s}(u_0(k) - R_s i_\alpha(k) - E_x(k)) + \dfrac{T_s}{L_s}u_\alpha(k) \\ \Delta i_\beta(k+1) = \dfrac{T_s}{L_s}(u_0(k) - R_s i_\beta(k) - E_x(k)) + \dfrac{T_s}{L_s}u_\beta(k) \end{cases} \tag{16}$$

where i_α, u_α, e_α and i_β, u_β, e_β are the current, voltage and back EMF in the stationary reference frame and α-β frame, respectively.

The left-hand side of equation defined as variation of current track can be changed by the right-hand side of equation. An active voltage vector is equal to itself adding zero vector. Therefore, the variations of current track consist of variations caused by zero voltage vector and active voltage vectors, which are represented by ($\Delta i_{\alpha 0}(k+1)$, $\Delta i_{\beta 0}(k+1)$) and ($\Delta i_{\alpha x}(k+1)$, $\Delta i_{\beta x}(k+1)$). As well-known, the six non-zero active voltage vectors are decided by the switching states of the inverter. When the dc-link voltage is constant, the amplitudes of six non-zero active voltage vectors are the same except the directions of them. If ignoring the variation of L_s and R_s, the amplitude of ($\Delta i_{\alpha x}(k+1)$, $\Delta i_{\beta x}(k+1)$) is also the same, other than the direction of ($\Delta i_{\alpha x}(k+1)$, $\Delta i_{\beta x}(k+1)$) resembling the applied active voltage vector. In order to reduce the computational burden aroused by the seven current tracks and cost function, a new reference frame α'-β' is established in this section. Use the transformation equation as the following:

$$\begin{cases} i_{\alpha'}(k+1) = i_\alpha(k) - i_{\alpha 0}(k+1) \\ i_{\beta'}(k+1) = i_\beta(k) + i_{\beta 0}(k+1) \end{cases} \tag{17}$$

where ($i_{\alpha'}(k+1)$, $i_{\beta'}(k+1)$ is the current track in the reference frame α'-β'.

The aim of establishing the frame α'-β' is to keep the current track generated by zero voltage vector in the frame α-β coinciding with the original point of the frame α'-β'. Therefore, the applied active voltage vector is reflected through the current track ($i_{\alpha'}(k+1)$, $i_{\beta'}(k+1)$) at horizontal and vertical coordinates ($\Delta i_{\alpha x}(k+1)$, $\Delta i_{\beta x}(k+1)$) in Fig. 5.

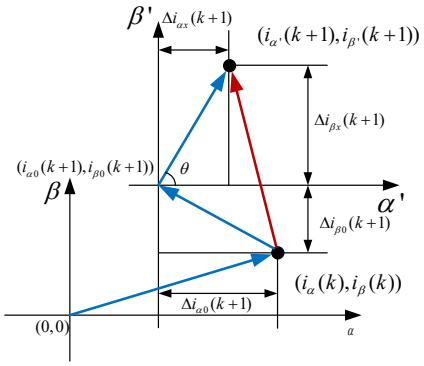

Fig. 5. Relative location of the new reference frame α'-β'and the stator reference frame α-β.

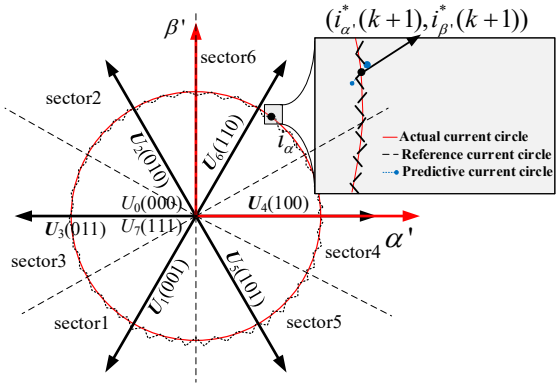

Fig. 6. Space voltage vector in the reference frame α'-β'.

In the reference frame α'-β', the whole region is also divided into six sectors (sector1-sector6) shown in Fig. 6. The direction of the current track is the same as the applied active voltage vector. The concrete position of current track is determined by the angle θ. According to the variation of current track caused by active voltage vectors, the value of tanθ can be

calculated. Because the angle range is fixed, the position of current track could be confirmed. Therefore, judging from the direction of the current track, the applied active voltage can be known.

After the selection of active voltage vector, the selection of zero voltage vector will relieve the torque ripple. The difference between the actual values of currents and the references in the reference frame α'-β' is obtained by (18), which is demonstrated in Fig. 7.

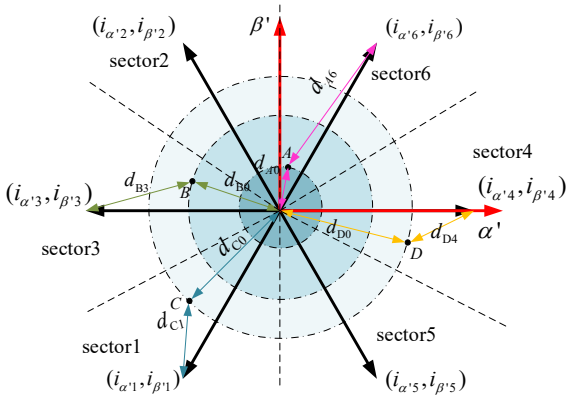

Fig. 7. Current track distribution in the reference frame α'-β'.

As can be seen, there are four typical current track points. If the zero voltage vectors are not considered, the active voltage vectors can be selected simply according to the positions A, B, C and D. The optimal active voltage vectors are u_6, u_3, u_1 and u_4, respectively. The distance can be calculated as the following:

$$\begin{cases} d_n = \sqrt{(i^*_{\alpha'} - i_{\alpha'})^2 + (i^*_{\beta'} - i_{\beta'})^2} \\ d_0 = \sqrt{(i^*_{\alpha'})^2 + (i^*_{\beta'})^2} \end{cases} \tag{18}$$

When ($i^*_{\alpha'}(k+1)$, $i^*_{\beta'}(k+1)$) is at point A, B, C or D in turn, d_{A0}, d_{B0}, d_{C0} and d_{D0} are the distances between the current track reference point and the original point of the frame α'-β', and d_{A6}, d_{B3}, d_{C1} and d_{D4} are the distances between current track reference point and actual current point, respectively. The smaller one will be used to select the corresponding voltage vector as the best voltage vectors. When the distances are equal to each other, they are defined as d_m. d_m is supposed as a constant value and determines whether or not active or zero voltage vectors should be selected. From the above analysis, d_0 is the distance between the current track point and the original point of the frame α'-β'. If d_0 is smaller than d_m, one zero voltage vector will be selected to keep the steady state performance, otherwise, one active voltage vector will be selected. With the increase of d_m, more and more zero voltage vectors will be selected to reduce the torque ripple. At typical current position B in Fig.7, d_{D0} can be assumed as the optimal value of d_m. The distance between the current track reference point and the original point of the frame α'-β' d_{B0} is equal to the distance between current track reference point and actual current point d_{B3}. The optimal vectors are consisted of u_3 and u_7, which divide the duration. In order to reduce the switch loss, only one bridge arm S_A is changed to produce fewer switching transitions.

The optimal value of d is obtained as:

$$d_{opt} = \frac{1}{2}\sqrt{u_\alpha(k)^2 + u_\beta(k)^2}\,\frac{T_s}{L_s} \tag{19}$$

Finally, the direction of the current track in the reference frame α'-β' is similar to that of the active voltage. The selection of the switching state for every sample period is based on the direction of the current track in Fig.8. The sampling frequency is different from the switching frequency. Because the continuous model needs to be transformed into discrete model. Therefore, the value of sampling frequency set in simulation determines the accuracy of the proposed strategy. The switching frequency depends on the electrical specification of power converter. The switching frequency setting in the RTI of dSPACE cannot surpass the maximum value of IGBT. The optimal vector duration is different in the sampling period, which will require the variable switching frequency. The duration is obtained by the amplitude and direct of reference current track in the reference frame α'-β'. As a result, the cost function is cancelled to reduce the computational burden.

Compared with the DCMPCC, the proposed MPCC has the following advantages. First, the methods of selecting optimal voltage vectors are different. In the duty-cycle-based MPCC, the optimal voltage vectors are composed of one active vector and one zero vector by cost function. In the proposed MPCC, the optimal voltage vector is selected based on the distance between the current track reference point and the original point of the frame α'-β' and the distance between current track reference point and actual current point. When the distances are equal to each other, they are defined as d_m. d_m is supposed as a constant value and determines whether or not active or zero voltage vectors should be selected. Second, only one active or zero voltage vector must be predicted to reduce the computation complexity in the proposed MPCC. Different points of reference current determine the different active or zero voltage vectors. Each point corresponds to a voltage vector, and more and more zero voltage vectors are selected with the increasing of d_m to reduce the torque ripples.

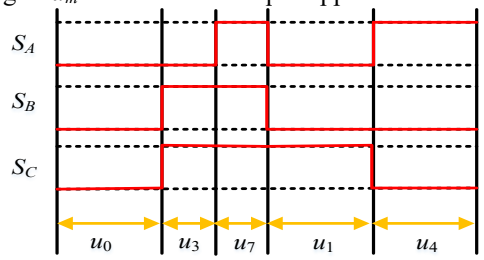

Fig. 8. Switching state for every sample of the points A, B, C, and D above.

IV. Simulation Results

To confirm the effectiveness of the proposed MPCC, the performance of the conventional MPCC, DCMPCC, and the proposed MPCC are compared in this section based on simulation results. The one-step delay caused by digital equipment has been compensated, and the sampling frequency of each method is set to 10 kHz. Table I lists the main parameters of the PMSM drive system.

A. Comparisons under speed change condition

For the simulation, two situations are considered for the

starting process, no-load and load, then speed/load changes are applied to the drive system to investigate the dynamic responses. Fig. 9 shows the dynamic responses of three control methods with no-load starting for the PMSM drive system. For each control method, three response curves are given. They are, from top to bottom, the rotor speed, electromagnetic torque and phase-A stator current. In the simulation, the initial reference speed for the starting process is 300 rpm, then a speed change (from 300 to 500 rpm) is applied at time 0.15 s and a load torque change (from 0 to 10 Nm) is applied at 0.35 s.

TABLE I
IPMSM DRIVE SYSTEM PARAMETERS

Parameter	Symbol	Value
Number of pole pairs	P	5
Stator resistance	R_s	0.18 Ω
d-axis inductance	L_d	0.174 mH
q-axis inductance	L_q	0.29 mH
Permanent-magnet flux linkage	ψ_f	0.0711 Wb
Inertia	J	0.067 kgm^2
Rated speed	N	2000 rpm
Rated power	P_N	60 kW

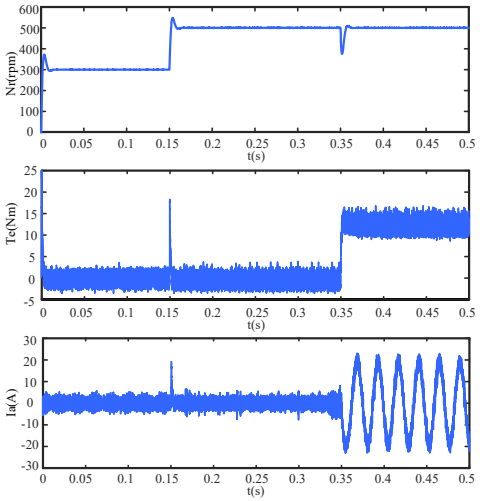

(a)

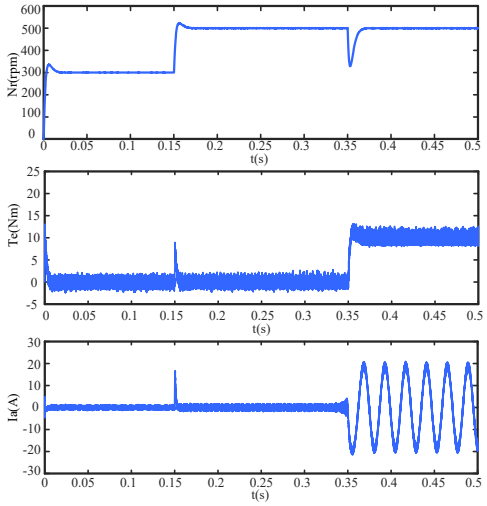

(b)

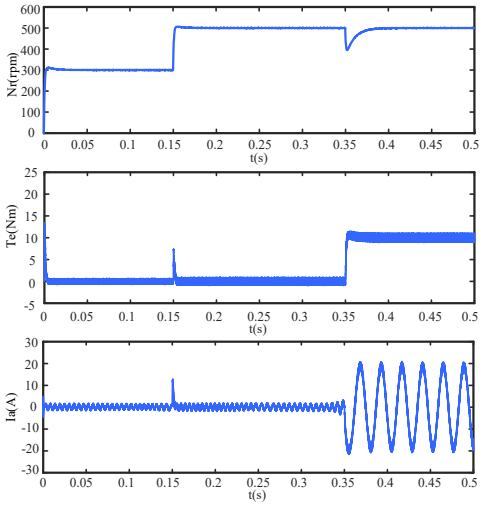

(c)

Fig. 9. Simulation starting response from standstill to 300 rpm with speed change: (a) Conventional MPCC, (b) DCMPCC, and (c) Proposed MPCC.

As shown, all three MPCC methods can reach the reference speed quickly. However, the conventional MPCC has a relatively large overshoot when the rotor speed reaches 300 rpm and changes to 500 rpm at 0.15 s. Meanwhile, the electromagnetic torque and phase current have significant oscillations. Fig. 10 shows total harmonic distortion (THD) of the current for three control methods. As shown, the current THDs of the three control methods are 17.4%, 3.58% and 1.42%, respectively. It can be seen that the proposed MPCC has the best performance in terms of steady state and dynamic response in this low-speed simulation because it has the lowest torque ripples and current harmonics.

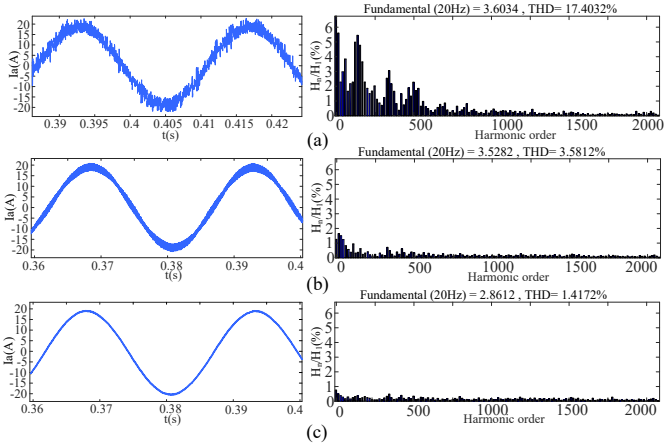

(a) (b) (c)

Fig. 10. Simulation current harmonic spectrum at 500 rpm with torque 10 Nm: (a) Conventional MPCC, (b) DCMPCC, and (c) Proposed MPCC.

B. Comparisons under torque change condition

Fig. 11 illustrates the dynamic responses of three control methods for the PMSM drive system with an initial load torque reference of 15 Nm and an initial reference speed of 2000 rpm. For each control method, three response curves are given as well. They are, from top to bottom, the rotor speed, electromagnetic torque and phase-A stator current. In the simulation, there are two changes for the load torque, i.e., from 15 to 0 Nm at 0.15 s and from 0 to 10 Nm at 0.35 s. As shown,

the DCMPCC and proposed MPCC present better dynamic and steady-state performance in terms of rotor speed, torque ripple and current harmonics than the conventional MPCC. Obviously, the proposed MPCC is more effective in reducing torque ripples and current harmonics.

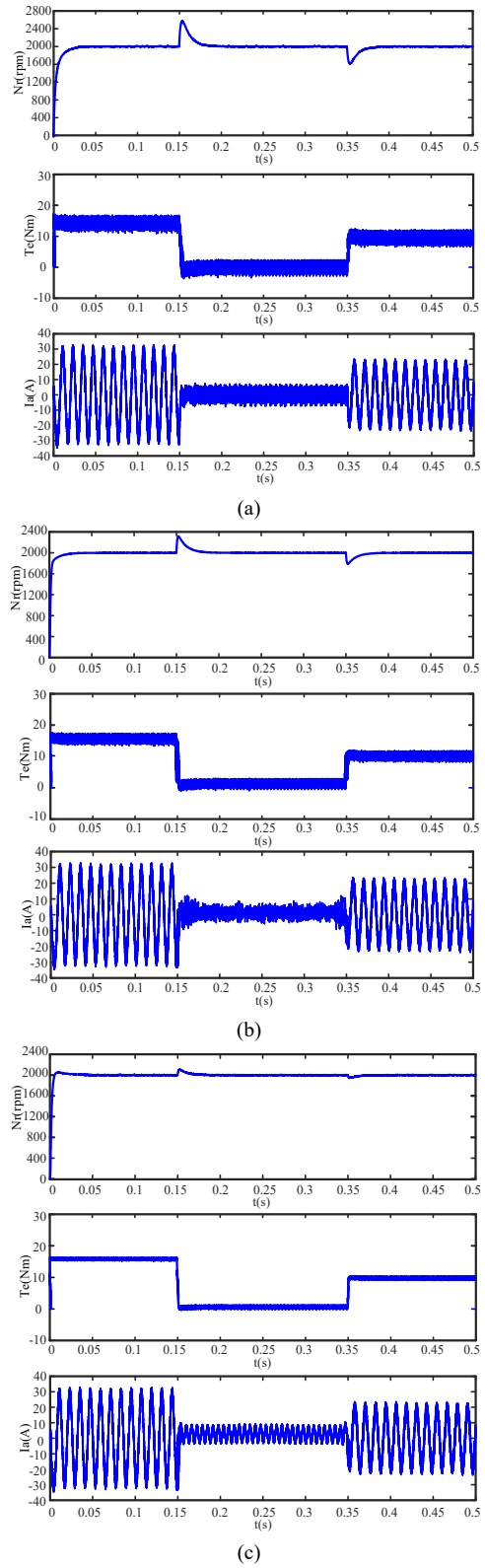

Fig. 11. Simulation starting response from standstill to 2000 rpm with load torque change: (a) Conventional MPCC, (b) DCMPCC, and (c) Proposed MPCC.

Fig. 12 shows the effectiveness of DCMPCC and the proposed MPCC in the reduction of current harmonics, under the condition of 15 Nm at 2000 rpm. The current THD is calculated up to 20 kHz. Apparently, the low-order harmonics in the DCMPCC and proposed MPCC are much lower than those in the conventional MPCC. The current THD of the conventional MPCC is 16.7%. It is higher than the values of DCMPCC (9.5%) and the proposed MPCC (3.5%). Again, the proposed MPCC has the smallest current harmonics.

The switching frequencies are determined by the requirements of software and hardware. In the RTI of dSPACE, the average switching frequencies are all set as 10 kHz, and they cannot surpass the maximum value of IGBT. It needs to sample at least once per period and then compute once. In theory, the higher sampling frequency, the more conducive to reduce latency and discretization error, but most commonly used controller computing power allows only switch cycle per sample and calculate the twice, the higher sampling frequency cannot complete the calculation of switch signal within a sampling period. Consequentially, the next sampling period will not be able to update the switch state. Hence, the sampling frequencies are equal to switching frequencies in this paper.

However, by counting the total switching steps during a short period, e.g., 0.05 s, it is found that the average switching frequencies of DCMPCC and the proposed MPCC at the steady state of 2000 rpm are much lower than 10 kHz. They can reduce switching loss effectively.

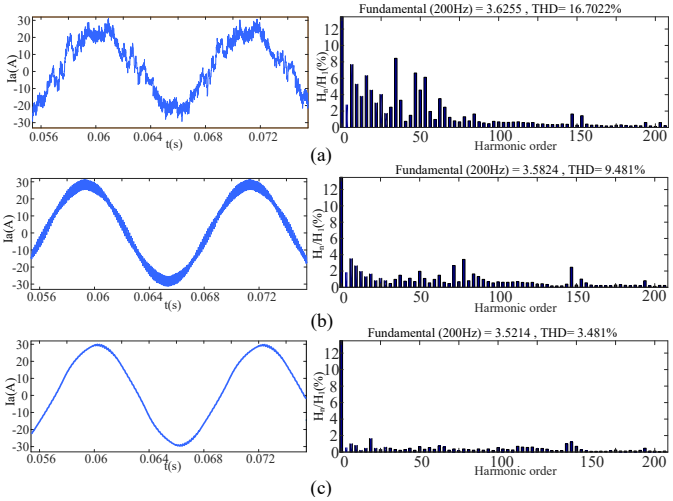

Fig. 12. Simulation current harmonic spectrum at 2000 rpm with torque 15 Nm: (a) Conventional MPCC, (b) DCMPCC, and (c) Proposed MPCC.

Comparing the THD both in low speed (300 to 500 rpm as shown in Fig. 10) and high speed (2000 rpm as shown in Fig. 12) ranges, it can be found that the performance in low speed is more remarkable. This is because the required voltage vector is small, and zero vectors are used in switching period for a long time at low speeds. The conventional MPCC only uses six basic voltage vectors, which cannot provide the required voltage vector. As for the proposed MPCC, active voltage vectors and zero voltage vectors are combined to obtain the required voltage vectors. Therefore, the proposed MPCC based on the current track circle can reach the optimal voltage vectors which yield low current harmonics and current THD.

C. Comparisons of converter output voltage

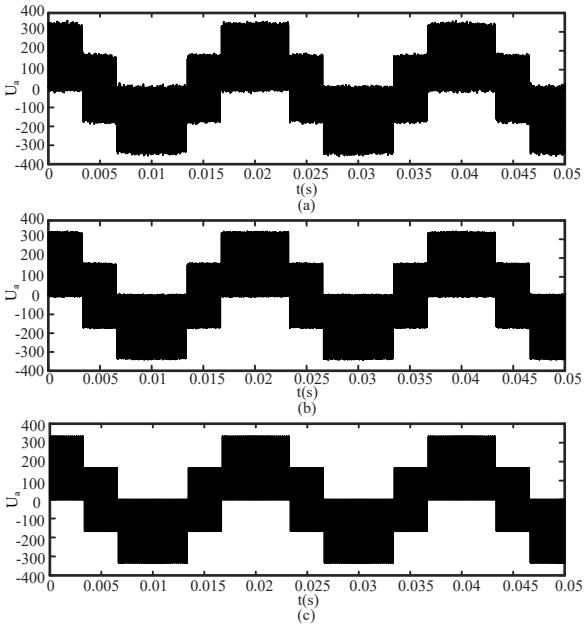

Fig. 13. Simulated converter output voltage for phase A: (a) Conventional MPCC, (b) DCMPCC, and (c) Proposed MPCC.

The simulated phase output voltage of the converter is shown in Fig. 13. Inverter's nonlinearity has influence on the motor performance, for the nonlinearity would result in harmonic components in the stator currents which certainly deteriorate the torque ripple. The sinusoidal alternating voltage is needed for PMSM drive which is generated by inverter. Therefore, the performance of steady and dynamic state is directly affected by the converter output voltage. Different control strategies have different effects on converter output voltage stability. It can be seen that the voltage controlled by the proposed MPCC has the best performance.

V. Experimental Results

In order to validate the simulation results, some experimental tests are carried out on a two-level inverter PMSM platform. Fig. 14 shows the experimental setup. The proposed control scheme is implemented in a dSPACE DS1007 PPC.

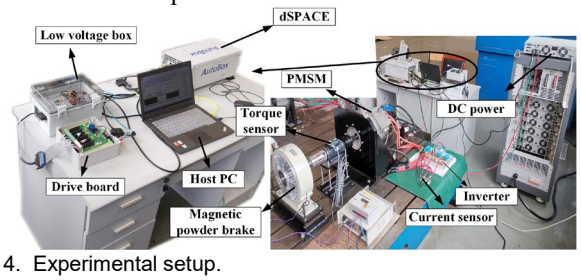

Fig. 14. Experimental setup.

Figs. 15 and 16 show the experimental results (the rotor speed, torque and phase-A stator current) of the PMSM with three MPCC methods. For the purposes of a smooth comparison, the same conditions are applied to obtain Fig. 15 and Fig. 9, i.e., starting with no-load, then a speed change at 0.15 s and a load torque change at 0.35 s. Similarly, same conditions are applied to obtain Fig. 11 and Fig. 16, i.e., starting with load, then two load torque changes at 0.15 and 0.35 s, respectively. The current waveform is given under the load torque 10 Nm in the experiment.

A. Comparisons under speed change condition

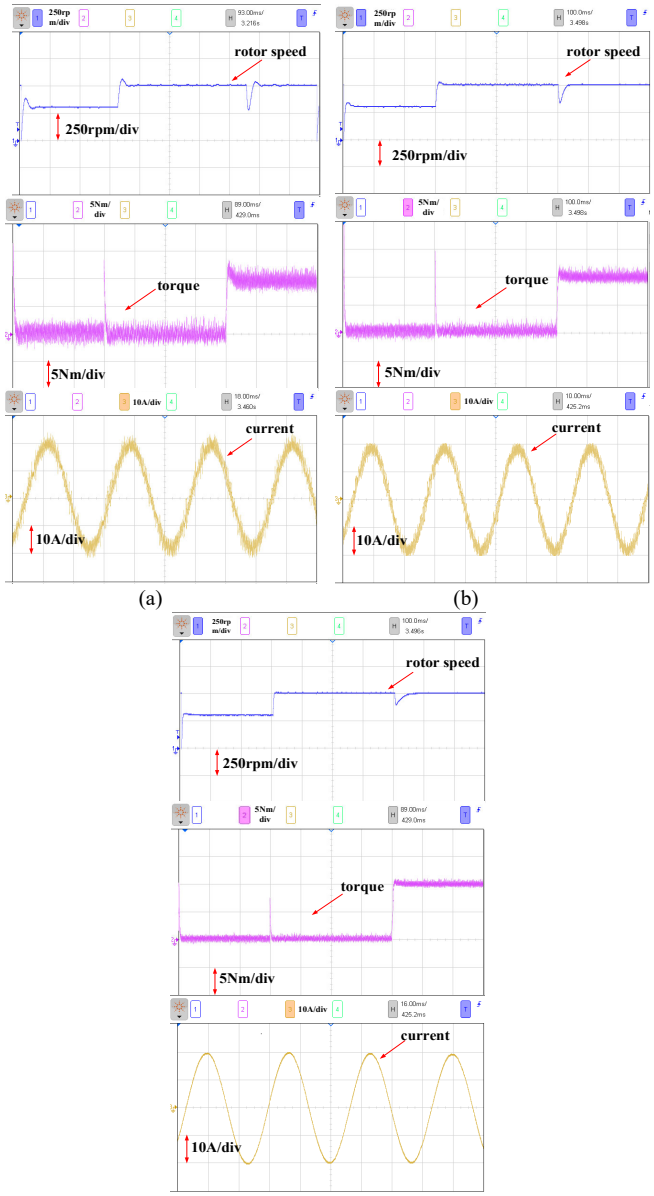

Fig. 15. Experimental starting response from standstill to 300 rpm with speed change: (a) Conventional MPCC, (b) DCMPCC, and (c) Proposed MPCC.

As shown in Fig. 15, all three MPCC methods can reach the reference speed quickly in this no-load starting process. However, the conventional MPCC has a relatively large overshoot when the rotor speed reaches 300 rpm and changes to 500 rpm. The dynamic performance of the proposed MPCC is the best. For the steady-state performance, the proposed MPCC has the best performance because it has the lowest torque ripples and current harmonics.

B. Comparisons under load change condition

As shown in Fig. 16, for a starting process with load and a higher initial reference speed, the DCMPCC and the proposed MPCC have better steady-state and dynamic performances than the conventional MPCC. The proposed MPCC is the best one

among them as it has the lowest speed overshoots, torque ripples, and current harmonics. Therefore, the advantages of the proposed MPCC have been confirmed by both simulation and experimental results.

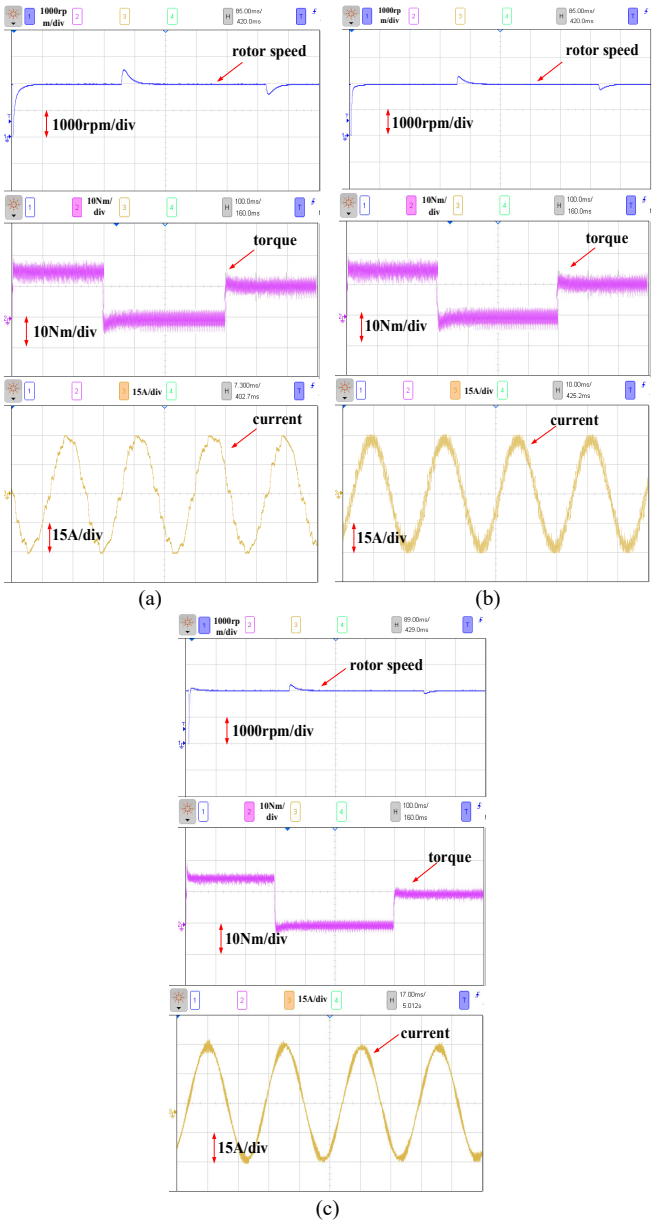

Fig. 16. Experimental starting response from standstill to 2000rpm with load torque change: (a) Conventional MPCC, (b) DCMPCC, and (c) Proposed MPCC.

C. Sensitivity analysis

Figs. 17-19 show the experimental results of motor speed response under the changes stator resistance, *d*-axis inductance, and *q*-axis inductance, respectively. In the experiment, ±50% step changes are applied to the stator resistance and *d*-*q* axis inductances at 0.22, 0.24 and 0.26 s. The motor runs at 2000 rpm for sensitivity analysis. As shown in Fig. 17, the variation of motor speed given by the proposed MPCC is much lower than that of the conventional MPCC under the change of the stator resistance. In the sensitivity test on the variation of inductance parameter, the proposed MPCC has a fluctuation but it reaches to stable state rapidly. In addition, the speed ripples have less impact compared to the high-speed drive. However, there are always fluctuations in the conventional MPCC. Therefore, the sensitivity analysis of the proposed MPCC and conventional MPCC are verified experimentally.

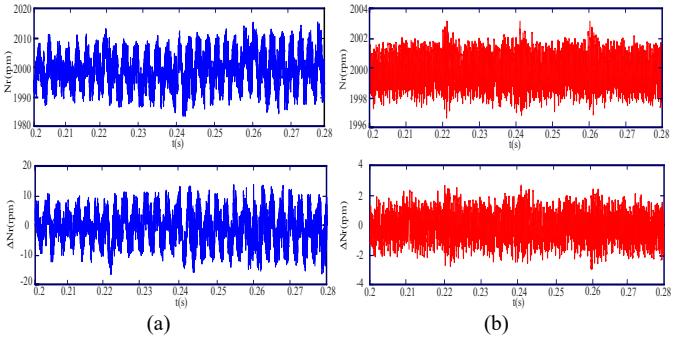

Fig. 17. Measured motor speed under the variation of stator resistance: (a) Conventional MPCC, (b) Proposed MPCC.

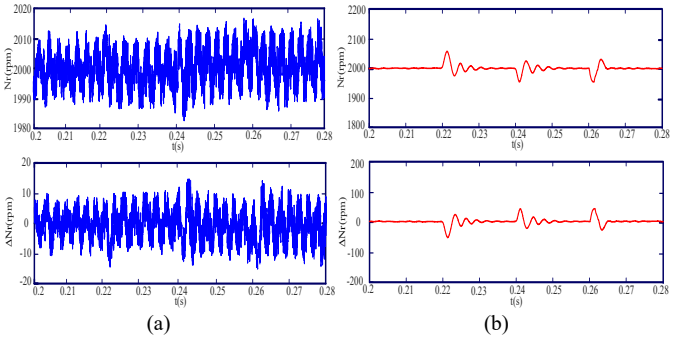

Fig. 18. Measured motor speed under the variation of *d*-axis inductance: (a) Conventional MPCC, (b) Proposed MPCC.

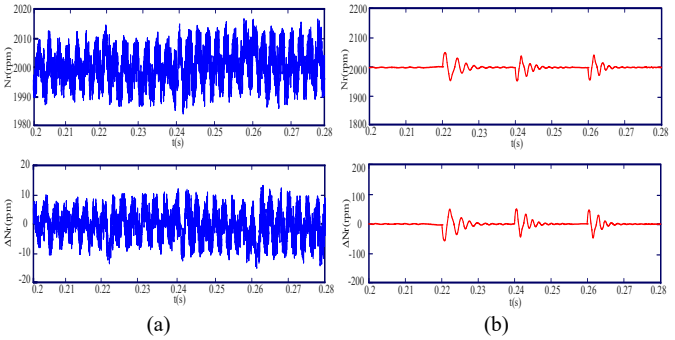

Fig. 19. Measured motor speed under the variation of *q*-axis inductance: (a) Conventional MPCC, (b) Proposed MPCC.

A steady-state performance comparison of the three methods is illustrated in Fig. 20. The comparison is divided into low speed and high-speed ranges. As can be seen, although the reduction of computation time is not significant between DCMPCC and the proposed MPCC, the torque ripples and current THDs are reduced significantly by using the proposed MPCC for both speed ranges. For the low-speed situation, the reduction of torque ripple and current THD are bigger than those for the high-speed situation, because the active voltage vectors and zero voltage vectors are combined to obtain the required voltage vectors more accurately in low speed. Moreover, the computation times of dSPACE for the conventional MPCC, DCMPCC and the proposed MPCC are 46.2, 35.4 and 32.1 μs, respectively at low speed, which are similar to those at high speed. Therefore, the proposed MPCC can reduce the computation time greatly compared with the conventional MPCC.

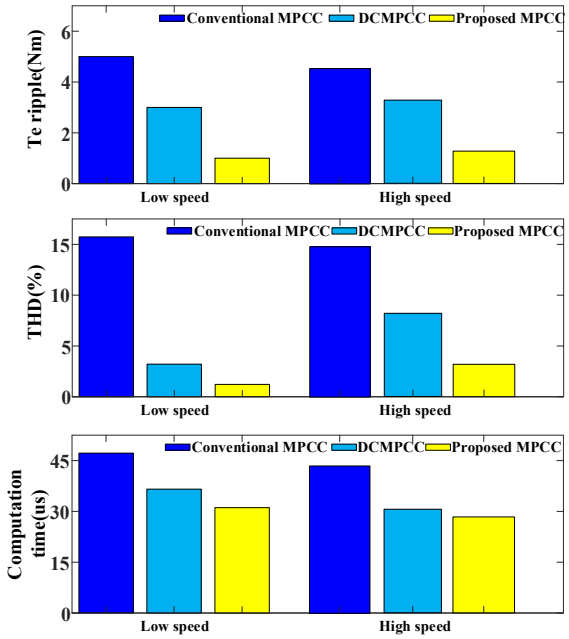

Fig. 20. Steady-state performance comparison in terms of torque ripple, current THD and computation time.

VI. Conclusion

This paper proposed an improved MPCC to effectively reduce the torque ripples and current harmonics of PMSM drives. In the study, the back EMF was estimated from the previous stator voltages and currents, and it was applied to predict the stator current in the next period. In order to reduce the computational burden, an improved MPCC was proposed with a new reference frame based on the prediction of the current track circle. The selection of the optimal voltage vector was based on the direction of the current track in the established reference frame instead of the cost function used in the conventional MPCC. The position of reference current in the established reference frame determines if the selection of zero voltage or active voltage can be selected as the optimal voltage vectors to obtain good driving performance. The advantages of the proposed MPCC were verified by comparative simulation and experiment results and the effect caused by the parameter mismatch is little.

References

[1] J. Lara, J. Xu, and A. Chandra, "Effects of rotor position error in the performance of field oriented controlled PMSM drives for electric vehicle traction applications," *IEEE Trans. Ind. Electron.*, vol.63, no 8, pp. 4738-4751, Aug. 2016.

[2] Z. Shi, X. Sun, Y. Cai, Z. Yang, G. Lei, Y. Guo, and J. Zhu, "Torque analysis and dynamic performance improvement of a PMSM for EVs by skew angle optimization," *IEEE Trans. Appl. Supercon.*, vol. 29, no. 2, Art. no. 0600305, Mar. 2019.

[3] A. Dalal and P. Kumar, "Design, prototyping, and testing of a dual-rotor motor for electric vehicle application," *IEEE Trans. Ind. Electron.*, vol. 65, no. 9, pp. 7185-7192, Sep. 2018.

[4] X. Sun, K. Diao, G. Lei, Y. Guo, and J. Zhu, "Study on segmented-rotor switched reluctance motors with different rotor pole numbers for BSG system of hybrid electric vehicles," *IEEE Trans on Veh. Technol.*, vol. 68, no. 6, pp. 5537-5547, Jun. 2019.

[5] X. Sun, Y. Shen, S. Wang, G. Lei, Z. Yang, and S. Han, "Core losses analysis of a novel 16/10 segmented rotor switched reluctance BSG motor for HEVs using nonlinear lumped parameter equivalent circuit model," *IEEE/ASME Trans. Mechatron.*, vol. 23, no. 2, pp. 747-757, Apr. 2018.

[6] X. Zhu, J. Huang, L. Quan, Z. Xiang, and B. Shi, "Comprehensive sensitivity analysis and multi-objective optimization research of permanent magnet flux-intensifying motors," *IEEE Trans. Ind. Electron.*, vol. 66, no. 4, pp. 2613-2627, Apr. 2019.

[7] X. Sun, J. Cao, G. Lei, Y. Guo, and J. Zhu, "Speed sensorless control for permanent magnet synchronous motors based on finite position set," *IEEE Trans. Ind. Electron.*, vol. 67, no. 7, pp. 6089-6100, Jul. 2020.

[8] J. Lara, J. Xu, and A. Chandra, "Effects of rotor position error in the performance of field oriented controlled PMSM drives for electric vehicle traction applications," *IEEE Trans. Ind. Electron.*, pp. 4738-4751, Aug. 2016.

[9] Z. Wang, J. Chen, M. Cheng, and K. T. Chau, "Field-oriented control and direct torque control for paralleled VSIs fed PMSM drives with variable switching frequencies," *IEEE Trans. Power Electron.*, vol. 31, no. 3, pp. 2417-2428, Mar. 2016.

[10] B. L. G. Costa, V. D. Bacon, S. A. O. da Silva, and B. A. Angélico, "Tuning of a PI-MR controller based on differential evolution metaheuristic applied to the current control loop of a Shunt-APF," *IEEE Trans. Ind. Electron*., vol. 64, no. 6, pp. 4751-4761, Jun. 2017.

[11] X. Sun, C. Hu, G. Lei, Y. Guo, and J. Zhu, "State feedback control for a PM hub motor based on grey wolf optimization algorithm," *IEEE Trans. Power Electron.*, vol. 35, no. 1, pp. 1136-1146, Jan. 2020.

[12] S. Yang, Y. Hsu, P. Chou, J. Chen, and G. Chen, "Digital implementation issues on high speed permanent magnet machine FOC drive under insufficient sample frequency," *IEEE Access.*, vol. 7, pp. 61484-61493, May. 2019.

[13] Z. Tang and B. Akin, "A new LMS algorithm based deadtime compensation method for PMSM FOC drives," *IEEE Trans. Ind. Appl.*, vol. 54, no. 6, pp. 6472-6484, Nov./Dec. 2018.

[14] Q. Liu and K. Hameyer, "Torque ripple minimization for direct torque control of PMSM with modified FCSMPC," *IEEE Trans. Ind. Appl.*, vol. 52, no. 6, pp. 4855-4864, Nov./Dec. 2016.

[15] A. Shinohara, Y. Inoue, S. Morimoto, and M. Sanada, "Maximum torque per ampere control in stator flux linkage synchronous frame for DTC-based PMSM drives without using q-Axis inductance," *IEEE Trans. Ind. Appl.*, vol. 53, no. 4, pp. 3663-3671, Jul./Aug. 2017.

[16] M. H. Vafaie, B. Mirzaeian Dehkordi, P. Moallem, and A. Kiyoumarsi, "A new predictive direct torque control method for improving both steady-state and transient-state operations of the PMSM," *IEEE Trans. Power Electron.*, vol. 31, no. 5, pp. 3738-3753, May. 2016.

[17] H. Nguyen and J. Jung, "Finite control set model predictive control to guarantee stability and robustness for surface-mounted PM synchronous motors," *IEEE Trans. Ind. Electron.*, vol. 65, no. 11, pp. 8510-8519, Nov. 2018.

[18] P. Kakosimos and H. Abu-Rub, "Predictive speed control with short prediction horizon for permanent magnet synchronous motor drives," *IEEE Trans. Power Electron.*, vol. 33, no. 3, pp. 2740-2750, Mar. 2018.

[19] X. Sun, *et al.*, "MPTC for PMSMs of EVs with multi-motor driven system considering optimal energy allocation," *IEEE Trans. Magn.*, vol. 55, no. 7, Art. no. 8104306, Jul. 2019.

[20] S. Wang, C. Li, C. Che, and D. Xu, "Direct torque control for 2L-VSI PMSM using switching instant table," *IEEE Trans. Power Electron.*, vol. 65, no. 12, pp. 9410-9420, Dec. 2018.

[21] X. Zhang, L. Zhang, and Y. Zhang, "Model predictive current control for PMSM drives with parameter robustness improvement," *IEEE Trans. Power Electron.,* vol. 34, no. 2, pp. 1645-1657, Feb. 2019.

[22] Y. Zhang, D. Xu, J. Liu, S. Gao, and W. Xu, "Performance improvement of model-predictive current control of permanent magnet synchronous motor drives," *IEEE Trans. Ind. Appl.,* vol. 53, no. 4, pp. 3683-3695, Jul./Aug. 2017.

[23] D. Zhou, S. Yang, and Y. Tang, "Model-predictive current control of modular multilevel converters with phase-shifted pulsewidth modulation," *IEEE Trans. Ind. Electron.,* vol. 66, no. 6, pp. 4368-4378, Jun. 2019.

[24] C. Lin, T. Liu, J. Yu, L. Fu, and C. Hsiao, "Model-free predictive current control for interior permanent-magnet synchronous motor drives based on current difference detection technique," *IEEE Trans. Ind. Electron.*, vol. 61, no. 2, pp. 667-681, Feb. 2014.

[25] X. Zhang and B. Hou, "Double vectors model predictive torque control without weighting factor based on voltage tracking error," *IEEE Trans. Power Electron.*, vol. 33, no. 3, pp. 2368-2380, Mar. 2018.

[26] L. Yan, M. Dou, Z. Hua, H. Zhang, and J. Yang, "Robustness improvement of FCS-MPTC for induction machine drives using disturbance feedforward compensation technique," *IEEE Trans. Power Electron.,* vol. 34, no. 3, pp. 2874-2886, Mar. 2019.

[27] Y. Zhou , H. Li , R. Liu, and J. Mao, "Continuous voltage vector model-free predictive current control of surface mounted permanent magnet synchronous motor," *IEEE Trans. Energy Conver.,* vol. 34, no. 2, pp. 899-908, Jun. 2019.
[28] C. Xiong, H. Xu, T. Guan, and P. Zhou, "A constant switching frequency multiple-vector-based model predictive current control of five-phase PMSM with nonsinusoidal back EMF," *IEEE Trans. Ind. Electron.*, vol. 67, no. 3, pp. 1695-1707, Mar. 2020.
[29] Y. Zhang, D. Xu, and L Huang, "Generalized multiple-vector-based model predictive control for PMSM drives," *IEEE Trans. Ind. Electron.*, vol. 65, no. 12, pp. 9356-9366, Dec. 2018.

Xiaodong Sun (M'12-SM'18) received the B.Sc. degree in electrical engineering, and the M.Sc. and Ph.D. degrees in control engineering from Jiangsu University, Zhenjiang, China, in 2004, 2008, and 2011, respectively.

Since 2004, he has been with Jiangsu University, where he is currently a Professor in Vehicle Engineering with the Automotive Engineering Research Institute. From 2014 to 2015, he was a Visiting Professor with the School of Electrical, Mechanical, and Mechatronic Systems, University of Technology Sydney, Sydney, Australia. His current teaching and research interests include electrical machines and drives, drives and control for electric vehicles, and intelligent control. He is the author or coauthor of more than 90 refereed technical papers and one book, and he is the holder of 36 patents in his areas of interest.

Minkai Wu was born in Suzhou, Jiangsu, China, in 1996. He received the B.S. degree in vehicle engineering from Yangzhou University, Yangzhou, China, in 2018, and he is currently working toward the M.E. degree in Vehicle Engineering in Jiangsu University, Zhenjiang, China.

His current research interests include control of electrical drive systems and advanced control strategy of electric machine.

Gang Lei (M'14) received the B.S. degree in Mathematics from Huanggang Normal University, China, in 2003, the M.S. degree in Mathematics and Ph.D. degree in Electrical Engineering from Huazhong University of Science and Technology, China, in 2006 and 2009, respectively. He is currently a senior lecturer in Electrical Engineering at the School of Electrical and Data Engineering, University of Technology Sydney (UTS), Australia. His research interests include design optimization and control of electrical drive systems and renewable energy systems.

Youguang Guo (S'02-M'05-SM'06) received the B.E. degree from Huazhong University of Science and Technology, China in 1985, the M.E. degree from Zhejiang University, China in 1988, and the Ph.D. degree from University of Technology, Sydney (UTS), Australia in 2004, all in electrical engineering. He is currently a Professor in Electrical Engineering at the School of Electrical and Data Engineering, University of Technology Sydney (UTS). His research fields include measurement and modeling of properties of magnetic materials, numerical analysis of electromagnetic field, electrical machine design optimization, power electronic drives and control.

Jianguo Zhu (S'93–M'96–SM'03) received the B.E. degree in 1982 from Jiangsu Institute of Technology, Jiangsu, China, the M.E. degree in 1987 from Shanghai University of Technology, Shanghai, China, and the Ph.D. degree in 1995 from the University of Technology Sydney (UTS), Sydney, Australia, all in electrical engineering. He was appointed a lecturer at UTS in 1994 and promoted to full professor in 2004 and Distinguished Professor of Electrical Engineering in 2017. At UTS, he has held various leadership positions, including the Head of School for School of Electrical, Mechanical and Mechatronic Systems and Director for Centre of Electrical Machines and Power Electronics. In 2018, he joined the University of Sydney, Australia, as a full professor and Head of School for School of Electrical and Information Engineering. His research interests include computational electromagnetics, measurement and modelling of magnetic properties of materials, electrical machines and drives, power electronics, renewable energy systems and smart micro grids.